

Chern dartboard insulator: sub-Brillouin zone topology and skyrmion multipoles

Yun-Chung Chen¹ , Yu-Ping Lin² & Ying-Jer Kao^{1,3,4} ✉

Topology plays a crucial role in many physical systems, leading to interesting states at the surface. A paradigmatic example is the Chern number defined in the Brillouin zone that leads to robust gapless edge states. Here we introduce the reduced Chern number, defined in the subregions of Brillouin zone, and construct a family of Chern dartboard insulators with quantized reduced Chern numbers but with trivial bulk topology. Chern dartboard insulators are protected by the mirror symmetries and exhibit distinct pseudospin textures, including (anti)skyrmions, inside the sub-Brillouin zone. These Chern dartboard insulators host exotic gapless edge states, such as Möbius fermions and midgap corner states, and can be realized in the photonic crystals. Our work opens up new possibilities for exploring sub-Brillouin zone topology and nontrivial surface responses in topological systems.

¹Department of Physics and Center for Theoretical Physics, National Taiwan University, Taipei 10607, Taiwan. ²Department of Physics, University of California, Berkeley 94720 CA, USA. ³Center for Quantum Science and Technology, National Taiwan University, Taipei 10607, Taiwan. ⁴National Center for High-Performance Computing, Hsinchu City 30076, Taiwan. ✉email: yjkao@phys.ntu.edu.tw

Chern insulators are classic examples of non-interacting systems with nontrivial bulk topology¹, where the quantized Hall conductivity is related to the first Chern number defined in the Brillouin zone (BZ)². The associated quantum anomalous Hall effect has been observed experimentally^{3–7} along with robust gapless edge states^{4,5,8,9}.

Recently, it is proposed that there exist a family of topological insulators with delicate topology protected by rotation symmetries^{10,11}. These systems have symmetric and exponentially-localized Wannier functions that cannot be entirely localized to δ -functions. This multicellular topology is shown to be a delicate property, where the topology can be trivialized by adding appropriate bulk atomic bands to either the conduction or valence bands¹¹. A related concept of noncompact atomic insulators is proposed¹², where certain obstructed atomic insulators with fragile complement cannot have orthonormal compact Wannier functions which are strictly local and have zero support outside a finite domain.

In this work, we show that nontrivial topology can appear locally in the BZ, even when the global topology is trivial. The idea relies on the concept of sub-Brillouin zone (sBZ) topology, where the topological invariant is defined in a fraction of the BZ. Consider a two-dimensional (2D) system with n mirror symmetries. The mirror symmetries divide the BZ into $2n$ sBZs with the high-symmetry lines (HSLs), which are the irreducible BZs in these systems. Based on these sBZs, we introduce a family of delicate topological systems, termed as the Chern dartboard insulators (CDIs). The n -th order CDIs (CDI _{n}) are defined with quantized first Chern numbers inside the irreducible BZs. Since the irreducible BZs are only $1/2n$ fraction of the BZ, all the CDIs exhibit sBZ topology. The n mirror symmetries protect the CDIs and the associated quantized reduced Chern numbers (Fig. 1a). These systems cannot be captured by the theories of tenfold way^{13,14}, symmetric indicators^{15–17} or topological quantum

chemistry^{18,19}. In addition, all the CDIs exhibit multicellular and even noncompact topology, i.e., the Wannier functions cannot be entirely localized to δ -functions due to the reduced Chern numbers.

Results

Theory. We aim at finding possible topology protected by n mirror symmetries $\mathcal{M}_1, \mathcal{M}_2, \dots, \mathcal{M}_n$. These symmetries divide the BZ into irreducible BZs, which become a fundamental domain to define the topology. A possible realization is to consider systems with the same mirror symmetry representation $\mathcal{M}_1, \dots, \mathcal{M}_n = \sigma_z \otimes I$,

$$\mathcal{M}_i H(\mathbf{k}) \mathcal{M}_i^{-1} = H(R_i \mathbf{k}), \quad (1)$$

where σ_z and I are the Pauli and identity matrices, and R_i 's represent the mirror reflections in the \mathbf{k} space. Here, the basis orbitals are chosen such that the mirror symmetry representation is diagonal. Therefore, the projection matrix onto the occupied space is block-diagonal at the HSLs. Notice that the system also has C_n symmetry with trivial representation $C_n = I$.

Next, we consider the models in which all the occupied states have the same mirror representations at the HSLs. The blocks in the projection matrix are thus composed of zero and identity matrices, which correspond to the unoccupied and occupied spaces, respectively. Up to a \mathbf{k} -dependent $U(1)$ phase, the HSLs are mapped onto a point in the Hilbert space. Note that the boundaries of irreducible BZs are composed of HSLs, or lines that can be mapped to each other by a C_n symmetry with trivial representation. Therefore, the irreducible BZs are topologically equivalent to a compact manifold. The first Chern number is

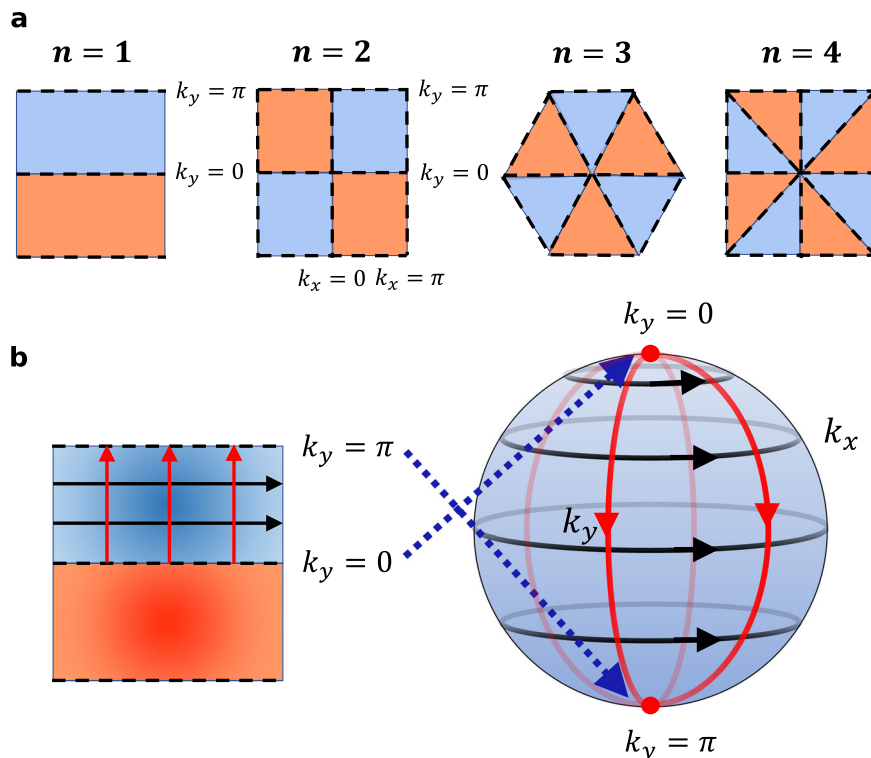


Fig. 1 Illustration of Chern dartboard insulators. **a** Chern dartboard insulators with different orders. The black dashed lines denote the high-symmetry lines of mirror symmetries in the Brillouin zone. The Chern number is quantized inside the regions enclosed by the high-symmetry lines. Here, the regions with blue and red color have reduced Chern number $C_n = 1, -1$ respectively. **b** Mercator projection of Type I $n = 1$ Chern dartboard insulator.

well-defined in the irreducible BZ

$$C_n = -\frac{1}{2\pi} \int_{\text{irBZ}} d^2k \text{Tr} F_{xy}. \quad (2)$$

Here F_{xy} is the non-Abelian Berry curvature, and C_n is the reduced Chern number of the n -th order CDIs.

The simplest CDI₁ is protected by one mirror symmetry and has quantized reduced Chern number inside half of the BZ. There are two types of CDI₁: Type I has opposite mirror representations at the two HSLs, which are positive and negative, respectively. A two-band tight-binding Hamiltonian with mirror symmetry $\mathcal{M}_y = \sigma_z$ serves as an example

$$H_1^I(\mathbf{k}) = \cos k_x \sin k_y \sigma_x + \sin k_x \sin k_y \sigma_y + (m + \cos k_y) \sigma_z. \quad (3)$$

In this model, the basis orbitals are an s and a p_y orbitals. The two HSLs at $k_y = 0, \pi$ divide the BZ into upper and lower sBZs. When $-1 < m < 1$, the upper and lower sBZs have quantized reduced Chern numbers $C_1 = \pm 1$, respectively. Note that the model hosts a flat-band limit at $m = 0$. If the total number of occupied bands is odd, Type I CDI₁ exhibits a quantized bulk polarization^{20–23}.

On the other hand, Type II CDI₁ has the same mirror representations at the two HSLs, which are either both positive or both negative. A flat-band model is given by

$$H_1^{II}(\mathbf{k}) = \frac{1}{2}(1 + \cos k_x) \sin 2k_y \sigma_x + \sin k_x \sin k_y \sigma_y + \frac{1}{2}[(1 + \cos k_x)(\cos 2k_y - 1) + 2] \sigma_z. \quad (4)$$

The bulk polarization $P_x = \int_0^{2\pi} \text{Tr} A_x dk_x$ shows the returning Thouless pump (RTP) behavior in both cases^{10,11}. The returning Thouless pump invariant is given by the difference of polarizations along the HSLs $\Delta P_x = P_x(k_y = \pi) - P_x(k_y = 0)$. Notably, this invariant is equivalent to the quantized reduced Chern number in the Type II CDI₁.

The sBZ topology can be visualized by mapping (3) to the Bloch sphere with $k_x \rightarrow \phi, k_y \rightarrow \theta$ ^{24,25}. This mapping is meaningful only when $k_y \in [0, \pi]$ or $k_y \in [-\pi, 0]$. In the Type I CDI₁, the upper sBZ is mapped to the entire sphere through the Mercator projection, thereby hosting the reduced Chern number $C_1 = 1$ (Figs. 1b and 2a). Meanwhile, the lower sBZ with $k_y \in [-\pi, 0]$ is also mapped to the entire sphere, but now with a negative reduced Chern number $C_1 = -1$ due to mirror symmetry. The quantization of these reduced Chern numbers can be understood as follows: Under the mirror symmetry $\mathcal{M}_y = \sigma_z$, the $k_y = 0$ and π HSLs are mapped to the north and south poles, respectively, as they have opposite representations. The sBZs are then topologically equivalent to S^2 , and the reduced Chern numbers C_1 are well-defined (Fig. 1b). In contrast to Type I CDI₁, Type II CDI₁ has well-defined skyrmions inside the sBZs, as shown in Fig. 2b. The sBZ topology is more complicated as both HSLs are mapped to the north pole, which can be directly related to the existence of skyrmions.

Higher-order CDIs are quite different from the CDI₁s, since they cannot be captured by the returning Thouless pump invariant. The connection of all HSLs enforces the same mirror-symmetry eigenvalues in the valence bands (or the conduction bands) among them. Therefore, the valence or conduction bands transform exactly the same as one of the trivial s or p orbitals with Wyckoff position a . Figures 2c–f and 3b plot the pseudospin textures of the two-band higher-order CDI _{n} s with $n = 2, 3, 4$. All these cases have blue-centered skyrmions or antiskyrmions inside the irreducible BZs, which lead to the nontrivial reduced Chern numbers $C_n = \pm 1$. With the proper definition from the irreducible BZ, the reduced Chern number

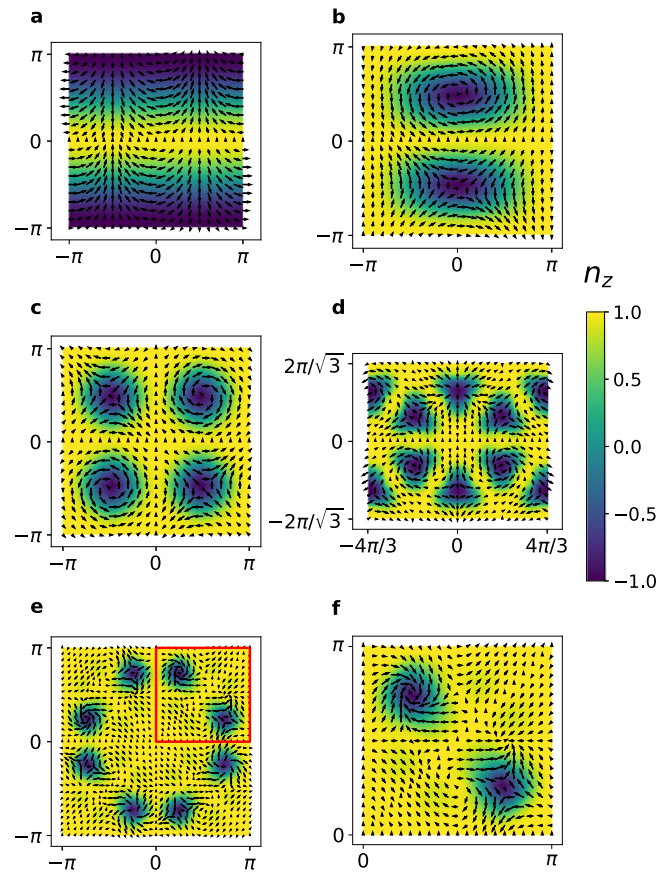


Fig. 2 Pseudospin textures of the Chern dartboard insulators. The vector field represents the components of n_x and n_y , and the color represents the n_z component. **a** Type I $n = 1$ Chern dartboard insulator in the flat-band limit. The reduced Chern number $C_1 = 1$ arising from the winding around the south pole at $k_y = \pi$. **b** Type II $n = 1$ Chern dartboard insulator in the flat-band limit. The reduced Chern number $C_1 = 1$ arising from the skyrmion living inside half of the BZ. **c** $n = 2$ Chern dartboard insulator. **d** Type I $n = 3$ Chern dartboard insulator. **e** $n = 4$ Chern dartboard insulator. **f** The zoom-in subplot for the red frame in **e**.

serves as a powerful generalization from the returning Thouless pump invariant.

Importantly, the mirror symmetry eigenvalues alone cannot detect CDIs. The CDIs are still inequivalent from the ones with δ -like Wannier functions, as they cannot be adiabatically transformed into each other. Moreover, the $n = 2, 4, 6$ CDIs are noncompact atomic insulators, where the orthonormal Wannier functions cannot be strictly local and compact¹². Note that these models are quite different from the noncompact cases studied in Ref. 12, where the noncompactness arises from the obstruction of the lattices that leads to obstructed atomic insulators. Here, the CDIs are not obstructed and the noncompactness arises due to the multicellularity. Also note that the CDI₅ does not exist since it is not lattice compatible.

There are also two types of CDI₃s. We define the Type I CDI₃ as the one with HSLs passing through the K and K' points (Fig. 1), and the Type II CDI₃ as the one with HSLs passing through the M and M' points (Fig. 3a). The Type II CDI₃ is slightly different from other CDIs. Here, the irreducible BZs are not enclosed by the HSLs (Fig. 3). Nevertheless, the lines $M' - K'$ and $M - K$ are mapped to each other by an emergent C_3 symmetry at the center of K or K' point. This C_3 symmetry is a combination of a C_3 symmetry (which comes from the three mirror symmetries) plus a \mathbf{k} -space translation. Therefore, the two

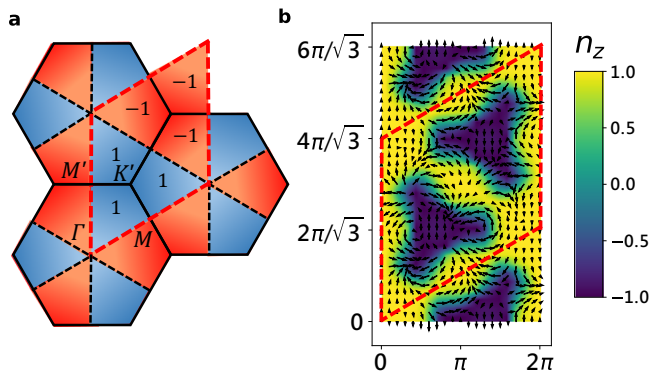


Fig. 3 Type II $n=3$ Chern dartboard insulator. **a** The quantized Chern number inside the irreducible BZs. The regions with blue and red color have reduced Chern number $C_n = 1, -1$ respectively. The dashed lines indicate the high-symmetry lines. The reciprocal lattice vectors $\mathbf{G}_1 = (2\pi, 2\pi/\sqrt{3})^T$ and $\mathbf{G}_2 = (0, 4\pi/\sqrt{3})^T$ form the rhombus-shape BZ, which is indicated by the red dashed lines. The numbers denote the Chern numbers inside the irreducible BZs, enclosed by the path $\Gamma - M' - K' - M - \Gamma$. **b** The pseudospin texture of the Type II $n=3$ Chern dartboard insulator. There are in total 6 skyrmions and 3 antiskyrmions inside half of the BZ, which add up to 3. The antiskyrmions are not clear in this figure since they are very close to the skyrmions.

boundary lines are glued together and effectively disappear. The sBZ topology is thus well-defined and Eq. (2) still applies. In particular, if we calculate the loop integral around the path $\Gamma - M' - K' - M - \Gamma$,

$$\frac{1}{2\pi} \int_{M'}^{K'} \mathbf{A} \cdot d\mathbf{k} + \frac{1}{2\pi} \int_{K'}^M \mathbf{A} \cdot d\mathbf{k} = 0 \quad (5)$$

due to the C_3 symmetry. The remaining integral

$$\frac{1}{2\pi} \int_{\Gamma}^{M'} \mathbf{A} \cdot d\mathbf{k} + \frac{1}{2\pi} \int_M^{\Gamma} \mathbf{A} \cdot d\mathbf{k} = -C_3 \in \mathbb{Z} \quad (6)$$

is a loop integral since M' maps to M by C_3 symmetry, which has a trivial representation. Therefore, the region enclosed by this path has a quantized reduced Chern number $C'_3 \in \mathbb{Z}$.

Gapless edge states. Similar to the Chern insulators, the appearance of gapless edge states in CDIs can be explained by the domain walls, with the exception of Type I CDI₁. Since the edges of CDIs serve as the boundaries between bulk and vacuum, domain walls naturally appear from the negative mass terms in the irreducible BZs under band inversions. For Type I CDI₁, there are no isolated band-inversion points. Therefore, the gapless edge states only exist in the directions perpendicular to the HSLs. On the other hand, the rest CDIs host isolated band-inversion points inside the irreducible BZ, owing to the quantized reduced Chern number C_n . Inside the irreducible BZ, the topology shares similar behavior with regular Chern insulators. If one tries to close the gap by creating massive Dirac cones at the band-inversion points, the minimal low-energy Dirac Hamiltonian with mirror symmetry representation $\sigma_z \otimes I$ can be expressed as

$$H(\mathbf{k}, r) = k_x \Gamma_x + k_y \Gamma_y + m(r) \sigma_z \otimes I, \quad (7)$$

where the three matrices $\Gamma_x, \Gamma_y, \sigma_z \otimes I$ anticommute with each other, and $m(r)$ is a position-dependent mass term. Since $m(r) < 0$ inside the bulk, gapless edge states appear as the domain walls between the bulk and the vacuum with $m(r) > 0$ ^{26,27}. In the two-band models, the band-inversion points are exactly associated with the skyrmion centers in Fig. 2.

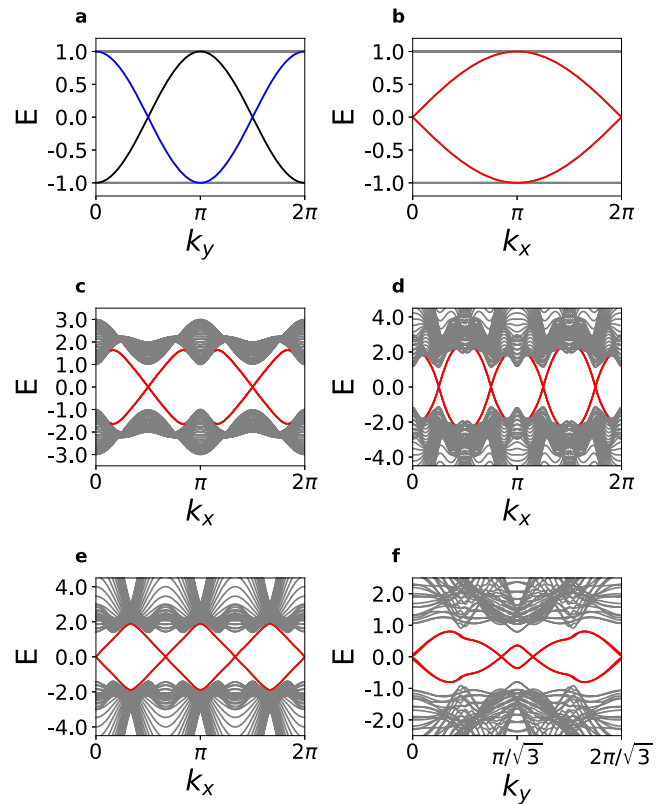


Fig. 4 Edge states of Chern dartboard insulators. The nanoribbon band structures are shown in all subfigures. The doubly degenerate edge states localized separately at the two opposite edges are highlighted by red color. **a** Type I and II $n=1$ Chern dartboard insulators with edges along the y -direction in the flat-band limit. The edge states localized at the left (right) edge are denoted by blue (black) color. **b** Type II $n=1$ Chern dartboard insulator with edges along the x -direction in the flat-band limit. **c** $n=2$ Chern dartboard insulator with edges along the x -direction. **d** $n=4$ Chern dartboard insulator with edges along the x -direction. **e** Type I $n=3$ Chern dartboard insulator with edges along the x -direction, which correspond to the flat edges. **f** Type II $n=3$ Chern dartboard insulator with edges along the y -direction, which correspond to the zigzag edges.

It is worth emphasizing a fundamental difference between the Chern insulators and the CDIs. In a Chern insulator with $C = 1$, we have only one band-inversion point inside the BZ. Thus, the chiral gapless edge states appear due to the domain walls between the bulk and the vacuum. However, for CDIs with $C_n = 1$, we have $2n$ band-inversion points with opposite-sign reduced Chern numbers. Therefore, we expect the edge states with opposite velocities in the edge spectrum. Following ref. ¹¹, we can derive the bulk-boundary correspondence

$$C_n = \frac{1}{n} \sum_j I\left(\frac{dE_j}{dk} > 0\right) = \frac{1}{n} \sum_j I\left(\frac{dE_j}{dk} < 0\right). \quad (8)$$

Here $I(x)$ is the indicator function counting the number of edge states, and dE_j/dk are the corresponding velocities. We have chosen an arbitrary energy level E that passes through the edge states, and the sum is over all the edge states. Since a positive reduced Chern number corresponds to an edge state with positive velocity (and vice versa), the bulk-boundary correspondence can be established accordingly. In Fig. 4, we plot the nanoribbon band structures for all the CDIs. Figure 4a represents the typical edge spectrum for delicate TIs. It is easy to observe that the bulk-boundary correspondence Eq. (8) is satisfied. Finally, the edge

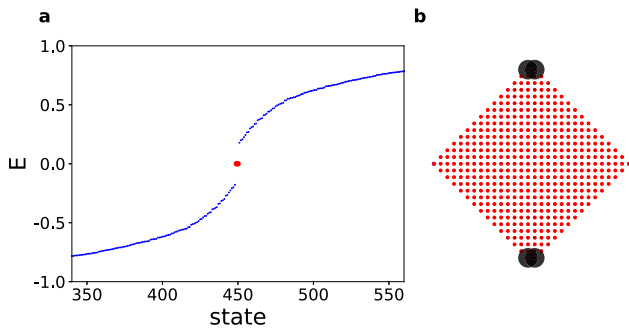


Fig. 5 Midgap corner states in Type I $n = 1$ Chern dartboard insulator.

a The nanoflake energy spectrum. **b** The probability distribution of the two corner states. In the flat-band limit, the left and right corners of the nanoflake also host midgap corner states, but they are not robust. Here for clarity, we set $m = 0.2$ and add the nearest-neighbor coupling $0.3 \cos k_x \sigma_z$ to Eq. (3).

states in Fig. 4c–f are doubly degenerate because of mirror symmetry that relates the two boundaries.

Midgap corner states. By cutting the edges along the (1,1) and (1,-1) directions of Type I CDI₁, we obtain two protected midgap corner states with quantized 1/2 charges. Notice that the unit cell is preserved, and the upper and lower corners have two atoms instead of one atom. Contrary to the 2D weak topological insulators where there are plenty of midgap edge states, Type I CDI₁ host two protected midgap corner states at the upper and lower corners (Fig. 5). This is similar to the midgap corner states in a model with quantized polarization²⁸, where the corner states appear along the polarization direction. Therefore, Type I CDI₁ also serves as the simplest two-band models with protected midgap corner states.

Möbius fermions. The edge states parallel to the x -axis in Type II CDI₁ show even more striking phenomenon. We expect two chiral gapless edge states with opposite chirality near $E = 0$, regardless of the edge terminations due to the band inversions inside the irreducible BZ. In the flat-band limit, the edge Hamiltonian describes the phase transition point of the four-band SSH model, and the edge states form the Möbius fermions²⁹ see Fig. 4b and Supplementary Note 1. The energy of the two edge states are $E_1(k_x) = \sin(k_x/2)$ and $E_2(k_x) = -\sin(k_x/2)$. A Möbius twist is clearly observed: The energies are only periodic in $k_x \in [0, 4\pi]$, and a single edge Dirac cone appears at $k_x = 0$. Since the edge Dirac cone is protected by the quantized reduced Chern number, the Dirac cone cannot disappear although the position can shift from $k_x = 0$. The $e^{ik_y/2}$ dependence is also clearly shown in the edge states. See Supplementary Note 1 for details. In addition to Type II CDI₁, the Möbius fermions also appear in both types of CDI₃s (Fig. 4e, f). See Supplementary note 2 for details. Finally, we note that the Möbius fermions can only appear with odd numbers of Dirac cones in the CDIs.

Discussion

We introduce the concept of sBZ topology that manifests itself in different classes of CDIs. CDIs host gapless edge states in general and can even develop nontrivial Möbius fermions or midgap corner states in certain cases. Although here we only consider specific examples of the sBZ topology, one can easily generalize the same argument to systems in higher dimensions or with different symmetries/constraints. The sBZ topology thus opens a fertile area for new topological systems with nontrivial surface responses. The different physical properties from the global

topology make the realization and classification of the sBZ topology a new frontier of research in topological materials.

We note that the concept of local topology has been discussed in the valley Hall effect and some attempts have been made to classify the topology^{30,31}. However, the valley Hall effect is not a robust band topology as (i) the valley Chern number is not exactly quantized (ii) the edge states can be trivialized by adiabatically transforming the Hamiltonian without closing the band gap. On the contrary, CDIs are systems with exactly quantized Chern number inside the sBZ and robust band topology. Finally, thanks to the recent advances in detecting local Berry curvature in various systems^{32,33}, and in realizing topological phases in nanophotonic silicon ring resonators³⁴, the realization and observation of CDIs and their exotic edge states is expected in the near future.

Methods

Conventions and definitions. With translational symmetry, the second quantized tight-binding Hamiltonian can be written into the Bloch form,

$$\hat{H} = \sum_{\mathbf{k}} c_{i,\mathbf{k}}^\dagger [H(\mathbf{k})]_{ij} c_{j,\mathbf{k}}, \quad (9)$$

where

$$c_{j,\mathbf{k}} = \frac{1}{\sqrt{N_t}} \sum_{\mathbf{R}} e^{i\mathbf{k} \cdot \mathbf{R}} c_{j,\mathbf{R}} \quad (10)$$

is the electron annihilation operator. Here, $j = 1, \dots, 2N$ labels the basis orbitals and spins, \mathbf{R} labels the unit cell position, and N_t is the total number of the unit cells. We use the convention that the Bloch Hamiltonian $H(\mathbf{k})$ is periodic under a translation of a reciprocal lattice vector \mathbf{G} :

$$H(\mathbf{k}) = H(\mathbf{k} + \mathbf{G}). \quad (11)$$

The intra-cell eigenstates are defined by:

$$H(\mathbf{k})|u^l(\mathbf{k})\rangle = E^l(\mathbf{k})|u^l(\mathbf{k})\rangle, \quad (12)$$

where $l = 1, \dots, 2N$ are the band indices and $E^l(\mathbf{k})$ is the eigenenergy. Note that one can generically choose a smooth and periodic gauge for the eigenstates of CDIs since the total Chern number is zero. Considering the half-filling band insulators, the intra-cell states can be decomposed into the valence states $|u_v^l\rangle$ and the conduction states $|u_c^l\rangle$, where $l = 1, \dots, N$. The Bloch state is given by $|\psi^l(\mathbf{k})\rangle = e^{i\mathbf{k} \cdot \mathbf{R}} |u^l(\mathbf{k})\rangle$.

The non-Abelian Berry connection for the valence bands is defined as:

$$A_{lm}(\mathbf{k}) = i\langle u_v^l(\mathbf{k}) | \nabla | u_v^m(\mathbf{k}) \rangle, \quad (13)$$

and the non-Abelian Berry curvature in two dimensions is:

$$F_{xy,lm} = \partial_x A_{y,lm} - \partial_y A_{x,lm} - i[A_x, A_y]_{lm}. \quad (14)$$

Mathematical formulation of Chern dartboard insulators.

Consider n mirror symmetries $\mathcal{M}_1, \mathcal{M}_2, \dots, \mathcal{M}_n$ with the same mirror symmetry representation $\mathcal{M}_1, \dots, \mathcal{M}_n = \sigma_z \otimes I$:

$$\mathcal{M}_i H(\mathbf{k}) \mathcal{M}_i^{-1} = H(R_i \mathbf{k}), \quad (15)$$

where R_i represent mirror reflections in \mathbf{k} space. Using Stokes theorem:

$$-\frac{1}{2\pi} \oint \text{Tr} \mathbf{A} \cdot d\mathbf{k} = -\frac{1}{2\pi} \int_{\text{irBZ}} d^2k \text{Tr} F_{xy} = C_n, \quad (16)$$

where \mathbf{A} and F_{xy} are the non-Abelian Berry connection and curvature, and C_n is the reduced Chern number of the n -th order CDIs. The loop integral encloses the irreducible BZ. On the HSLs,

the valence states are eigenstates of the Hamiltonian due to Eq. (15). Next, we consider the models where all the occupied states at the high-symmetry lines have the same mirror representations. As a result, the valence states are spanned by the basis orbitals:

$$|u_v^i(\mathbf{k} \in \text{HSLs})\rangle = \sum_{j=1}^N U_{ij}(\mathbf{k} \in \text{HSLs}) |b^j\rangle, \quad (17)$$

where $|b^j\rangle$ with $j = 1, \dots, N$ are the basis orbitals that have the same mirror symmetry representation with the occupied states $|u_v^i(\mathbf{k} \in \text{HSLs})\rangle$. Here, the basis orbitals are chosen into the basis such that the mirror symmetry representation is diagonal. Since the total Chern number is zero, $U_{ij}(\mathbf{k})$ can be chosen to a smooth and periodic $U(N)$ gauge transformation. The key point is that the rank of the occupied states is equal to the rank of the basis states $|b^j\rangle$ such that $U_{ij}(\mathbf{k})$ is a well-defined $U(N)$ gauge transformation. By plugging Eq. (17) into Eq. (16), it follows that,

$$\frac{i}{2\pi} \int \text{Tr}[U_\pi^\dagger \nabla U_\pi - U_0^\dagger \nabla U_0] \cdot d\mathbf{k} = C_1, \quad (18)$$

where U_π and U_0 denote the gauge transformation at the two different HSLs, and

$$-\frac{i}{2\pi} \oint \text{Tr} U^\dagger \nabla U \cdot d\mathbf{k} = C_n, \quad (19)$$

for $n > 1$. The reduced Chern number is thus quantized to integers. Note that the \mathbf{k} -dependent $U(1)$ phase is crucial to obtain the nonzero reduced Chern number.

Skyrmion number. The topology of two-band CDIs can be visualized using the pseudospin textures. We first expand the Bloch Hamiltonian into the Pauli matrices:

$$H(\mathbf{k}) = \sum_i d_i(\mathbf{k}) \sigma_i, \quad (20)$$

where σ_i with $i = x, y, z$ are the Pauli matrices. The reduced Chern number can be defined as the degree of the map from the irreducible BZ to S^2 :

$$C_n = -\frac{1}{4\pi} \int_{\text{irBZ}} d^2\mathbf{k} n \cdot \left(\frac{\partial \mathbf{n}}{\partial k_x} \times \frac{\partial \mathbf{n}}{\partial k_y} \right) \quad (21)$$

where $\mathbf{n}(\mathbf{k}) = \mathbf{d}(\mathbf{k})/|\mathbf{d}(\mathbf{k})|$ are the unit vectors that define the space of S^2 . The reduced Chern number measures how many times the irreducible BZ wraps around S^2 .

The pseudospin textures of CDIs are plotted in Fig. 2. The first Chern number can be calculated as the sum of the indices around either $\mathbf{n}_0 = (0, 0, 1)$ or $\mathbf{n}_0 = (0, 0, -1)$ inside the BZ, with a sign difference³⁵. Note that this choice is just for convenience as one can easily do an arbitrary unitary transformation. The reduced Chern number is

$$C_n = \sum_i S_i, \quad (22)$$

where S_i is the index around the south pole $\mathbf{n}_0 = (0, 0, -1)$ with the blue center in the plot, and i denotes the different skyrmions inside the BZ. Since the irreducible BZ is a two-dimensional manifold, the indices can be calculated simply as the winding numbers of the vectors around the south pole. Notice that the Poincaré-Hopf theorem constrains the total indices including those around the north pole $\mathbf{n}_0 = (0, 0, 1)$ are summed to zero. This is consistent with Eq. (21) since a nonzero Chern number implies the north pole and the south pole must be wrapped around nontrivially.

Tight-binding models. Here we list the two-band spinless tight-binding models used to construct the figures in the main text for CDIs. The $n = 1, 2, 4$ CDIs are built in the simple square lattice

with primitive lattice vectors $\mathbf{a}_1 = (1, 0)$ and $\mathbf{a}_2 = (0, 1)$ in the unit of a lattice constant. The CDI₃ is built in the triangular lattice with primitive lattice vectors $\mathbf{a}_1 = (1, 0)$ and $\mathbf{a}_2 = (1/2, \sqrt{3}/2)$ in the unit of a lattice constant. The basis orbitals are all placed on the atoms. The numerical results of the midgap corner states and the nanoribbon band structures are performed using the P_{YTH}TB package³⁶.

Type I CDI₁:

$$H_1^I(\mathbf{k}) = \cos k_x \sin k_y \sigma_x + \sin k_x \sin k_y \sigma_y + (m + \cos k_y) \sigma_z, \quad (23)$$

where m is a parameter. The basis orbital consists of a s orbital and a p_y orbital. The Hamiltonian has the mirror symmetry $\mathcal{M}_y = \sigma_z$. For $-1 < m < 1$, this model has a quantized reduced Chern number $C_1 = 1$ inside the upper half BZ, see Fig. 1. The system has a flat-band limit when $m = 0$.

Type II CDI₁:

$$H_1^{II}(\mathbf{k}) = \cos k_x \sin 2k_y \sigma_x + \sin k_x \sin k_y \sigma_y + (m + \cos 2k_y - \cos k_x) \sigma_z, \quad (24)$$

where m is a parameter. The basis orbital consists of a s orbital and a p_y orbital. The Hamiltonian has the mirror symmetry $\mathcal{M}_y = \sigma_z$. For $0 < m < 2$, this model has a quantized reduced Chern number $C_1 = 1$ inside the upper half BZ, see Fig. 1. The system has a flat-band limit in the following form:

$$H_1^{IIc}(\mathbf{k}) = \frac{1}{2} (1 + \cos k_x) \sin 2k_y \sigma_x + \sin k_x \sin k_y \sigma_y + \frac{1}{2} [(1 + \cos k_x)(\cos 2k_y - 1) + 2] \sigma_z. \quad (25)$$

CDI₂:

$$H_2(\mathbf{k}) = -\sin k_x \sin 2k_y \sigma_x + \sin 2k_x \sin k_y \sigma_y + (m + \cos 2k_x + \cos 2k_y) \sigma_z. \quad (26)$$

where m is a parameter. The basis orbital consists of a s orbital and a d_{xy} orbital. The Hamiltonian has two mirror symmetries $\mathcal{M}_x = \mathcal{M}_y = \sigma_z$. For $0 < m < 2$, this model has a quantized reduced Chern number $C_2 = 1$ inside the upper right quarter of the BZ, see Fig. 1. We set $m = 1.0$ for all the figures.

CDI₄:

$$H_4(\mathbf{k}) = \left(-\sin k_x \sin 4k_y + \sin 4k_x \sin k_y \right) \sigma_x + \left(\sin 2k_x \sin 4k_y - \sin 4k_x \sin 2k_y \right) \sigma_y + \left[m + \cos 2k_x + \cos 2k_y + \cos 4k_x + \cos 4k_y + 4 \cos k_x \cos k_y \right] \sigma_z, \quad (27)$$

where m is a parameter. The basis orbital consists of a s orbital and a second orbital that is odd under four mirror symmetries. The Hamiltonian has four mirror symmetries $\mathcal{M}_x = \mathcal{M}_y = \mathcal{M}_{x+y} = \mathcal{M}_{x-y} = \sigma_z$. For $2 < m < 4$, this model has a quantized reduced Chern number $C_4 = 1$ inside the irreducible BZ, see Fig. 1. We set $m = 3.0$ for all the figures.

Type I CDI₃:

$$H_3(\mathbf{k}) = \left[\sin \frac{5}{2} k_x \sin \frac{\sqrt{3}}{2} k_y - \sin 2k_x \sin \sqrt{3} k_y \right. \\ \left. + \sin \frac{1}{2} k_x \sin \frac{3\sqrt{3}}{2} k_y \right] \sigma_x \\ + \left[-\cos \frac{5}{2} k_x \sin \frac{\sqrt{3}}{2} k_y - \cos 2k_x \sin \sqrt{3} k_y \right. \\ \left. + \cos \frac{1}{2} k_x \sin \frac{3\sqrt{3}}{2} k_y \right] \sigma_y \\ + \left[m + \sum_{a=1}^6 \left(e^{it_2(a) \cdot \mathbf{k}} + \frac{1}{2} e^{2it_2(a) \cdot \mathbf{k}} \right) \right] \sigma_z, \quad (28)$$

where m is a parameter and $\mathbf{t}_2(a) = \sqrt{3}[\cos(\pi a/3 - \pi/6), \sin(\pi a/3 - \pi/6)]^T$. The basis orbitals consist of a s orbital and a $f_{y(3x^2-y^2)}$ orbital. The Hamiltonian has three mirror symmetries $\mathcal{M}_y = C_3 \mathcal{M}_y C_3^{-1} = C_3^2 \mathcal{M}_y C_3^{-2} = \sigma_z$. The σ_z term contains the hoppings with range $\mathbf{a}_1 + \mathbf{a}_2$, $2(\mathbf{a}_1 + \mathbf{a}_2)$, and also the ones generated by all the C_6 rotations. The σ_x and σ_y terms contain the hoppings with range $\mathbf{a}_1 + 2\mathbf{a}_2$ and the ones generated by three mirror symmetries. For $0 < m < 4.5$, this model has a quantized reduced Chern number $\mathcal{C}_3 = 1$ inside the irreducible BZ, see Fig. 1. We set $m = 2.0$ for all the figures.

Type II CDI₃:

$$H_3^{\text{II}}(\mathbf{k}) = \left[\sin \frac{5}{2} k_x \sin \frac{\sqrt{3}}{2} k_y - \sin 2k_x \sin \sqrt{3} k_y \right. \\ \left. + \sin \frac{1}{2} k_x \sin \frac{3\sqrt{3}}{2} k_y \right] \sigma_x \\ + \left[\sin \frac{5}{2} k_x \cos \frac{\sqrt{3}}{2} k_y - \sin 2k_x \cos \sqrt{3} k_y \right. \\ \left. - \sin \frac{1}{2} k_x \cos \frac{3\sqrt{3}}{2} k_y \right] \sigma_y \\ + \left[m + \sum_{a=1}^6 \left(e^{it_1(a) \cdot \mathbf{k}} + e^{2it_1(a) \cdot \mathbf{k}} \right) \right] \sigma_z, \quad (29)$$

where m is a parameter and $\mathbf{t}_1(a) = [\cos(\pi a/3), \sin(\pi a/3)]^T$. The basis orbitals consist of a s orbital and a $f_{x(x^2-3y^2)}$ orbital. The Hamiltonian has three mirror symmetries $\mathcal{M}_x = C_3 \mathcal{M}_x C_3^{-1} = C_3^2 \mathcal{M}_x C_3^{-2} = \sigma_z$. The σ_z term contains the hoppings with range \mathbf{a}_1 , $2\mathbf{a}_1$, and also the ones generated by all the C_6 rotations. The σ_x and σ_y contains the hoppings with range $2\mathbf{a}_1 + \mathbf{a}_2$ and the ones generated by three mirror symmetries. The system has a quantized reduced Chern number $\mathcal{C}_3 = 1$ if $0.5 < m < 2.5$, see Fig. 3. We set $m = 1.5$ for all the figures.

Data availability

The data for all the figures are open at this website: https://github.com/clock871225/Chern_dashboard_insulator.

Received: 27 March 2023; Accepted: 13 December 2023;

Published online: 15 January 2024

References

- Haldane, F. D. M. Model for a quantum Hall effect without Landau levels: condensed-matter realization of the “parity anomaly”. *Phys. Rev. Lett.* **61**, 2015–2018 (1988).
- Qi, X.-L., Wu, Y.-S. & Zhang, S.-C. Topological quantization of the spin Hall effect in two-dimensional paramagnetic semiconductors. *Phys. Rev. B* **74**, 085308 (2006).

- Chang, C.-Z. et al. Experimental Observation of the Quantum Anomalous Hall Effect in a Magnetic Topological Insulator. *Science* **340**, 167–170 (2013).
- Liu, C.-X., Zhang, S.-C. & Qi, X.-L. The Quantum Anomalous Hall Effect: Theory and Experiment. *Annu. Rev. Condens. Matter Phys.* **7**, 301–321 (2016).
- He, K., Wang, Y. & Xue, Q.-K. Topological Materials: Quantum Anomalous Hall System. *Annu. Rev. Condens. Matter Phys.* **9**, 329–344 (2018).
- Deng, Y. et al. Quantum anomalous Hall effect in intrinsic magnetic topological insulator MnBi_2Te_4 . *Science* **367**, 895–900 (2020).
- Serlin, M. et al. Intrinsic quantized anomalous Hall effect in a moiré heterostructure. *Science* **367**, 900–903 (2020).
- Kitaev, A. Periodic table for topological insulators and superconductors. *AIP Conf. Proc.* **1134**, 22–30 (2009).
- Ryu, S., Schnyder, A. P., Furusaki, A. & Ludwig, A. W. W. Topological insulators and superconductors: tenfold way and dimensional hierarchy. *N. J. Phys.* **12**, 065010 (2010).
- Kruthoff, J., de Boer, J., van Wezel, J., Kane, C. L. & Slager, R.-J. Topological Classification of Crystalline Insulators through Band Structure Combinatorics. *Phys. Rev. X* **7**, 041069 (2017).
- Po, H. C., Vishwanath, A. & Watanabe, H. Symmetry-based indicators of band topology in the 230 space groups. *Nat. Commun.* **8**, 50 (2017).
- Po, H. C. Symmetry indicators of band topology. *J. Phys. Condens. Matter* **32**, 263001 (2020).
- Bradlyn, B. et al. Topological quantum chemistry. *Nature* **547**, 298–305 (2017).
- Cano, J. et al. Building blocks of topological quantum chemistry: Elementary band representations. *Phys. Rev. B* **97**, 035139 (2018).
- Benalcazar, W. A., Bernevig, B. A. & Hughes, T. L. Electric multipole moments, topological multipole moment pumping, and chiral hinge states in crystalline insulators. *Phys. Rev. B* **96**, 245115 (2017).
- Benalcazar, W. A., Bernevig, B. A. & Hughes, T. L. Quantized electric multipole insulators. *Science* **357**, 61–66 (2017).
- Benalcazar, W. A., Li, T. & Hughes, T. L. Quantization of fractional corner charge in C_n -symmetric higher-order topological crystalline insulators. *Phys. Rev. B* **99**, 245151 (2019).
- Schindler, F. et al. Fractional corner charges in spin-orbit coupled crystals. *Phys. Rev. Res.* **1**, 033074 (2019).
- Alexandradinata, A. A topological principle for photovoltaics: Shift current in intrinsically polar insulators. Preprint at <https://arxiv.org/abs/2203.11225> (2022).
- Zhu, P., Noh, J., Liu, Y. & Hughes, T. L. Scattering theory of delicate topological insulators. *Phys. Rev. B* **107**, 195110 (2023).
- Hasan, M. Z. & Kane, C. L. Colloquium: Topological insulators. *Rev. Mod. Phys.* **82**, 3045–3067 (2010).
- Su, W. P., Schrieffer, J. R. & Heeger, A. J. Soliton excitations in polyacetylene. *Phys. Rev. B* **22**, 2099–2111 (1980).
- Ezawa, M. Higher-Order Topological Insulators and Semimetals on the Breathing Kagome and Pyrochlore Lattices. *Phys. Rev. Lett.* **120**, 026801 (2018).
- Shiozaki, K., Sato, M. & Gomi, K. Z_2 topology in nonsymmorphic crystalline insulators: Möbius twist in surface states. *Phys. Rev. B* **91**, 155120 (2015).
- Mañes, J. L. Existence of bulk chiral fermions and crystal symmetry. *Phys. Rev. B* **85**, 155118 (2012).
- Saba, M. et al. Nature of topological protection in photonic spin and valley Hall insulators. *Phys. Rev. B* **101**, 054307 (2020).
- Wimmer, M., Price, H. & Carusotto, I. Experimental measurement of the Berry curvature from anomalous transport. *Nat. Phys.* **13**, 545–550 (2017).
- Schüler, M. et al. Local Berry curvature signatures in dichroic angle-resolved photoelectron spectroscopy from two-dimensional materials. *Sci. Adv.* **6**, eaay2730 (2020).
- Leykam, D. & Yuan, L. Topological phases in ring resonators: recent progress and future prospects. *Nanophotonics* **9**, 4473–4487 (2020).
- von Gersdorff, G., Panahiyan, S. & Chen, W. Unification of topological invariants in Dirac models. *Phys. Rev. B* **103**, 245146 (2021).
- Python tight binding open-source package, <http://www.physics.rutgers.edu/pythtb/> (2016).

Acknowledgements

The authors thank Yi-Chun Hung for helpful discussions. Y.C.C. and Y.J.K. were partially supported by the National Science and Technology Council of Taiwan under grants No. 108-2112-M-002-020-MY3, 110-2112-M-002-034-MY3, 111-2119-M-007-009, and by the National Taiwan University under Grant No. NTU-CC-111L894601. Y.P.L. received the fellowship support from the Emergent Phenomena in Quantum Systems (EPiQS) program of the Gordon and Betty Moore Foundation. This research was supported in part by the National Science Foundation under Grants No. NSF PHY-1748958 and PHY-2309135.

Author contributions

Y.C.C. conceived the ideas and performed the theoretical and numerical analysis. Y.P.L. provided the idea to look at the pseudospin textures and Möbius fermions. Y.J.K. supervised the project. Y.C.C., Y.P.L. and Y.J.K. wrote the manuscript.

Competing interests

The authors declare no competing interests.

Additional information

Supplementary information The online version contains supplementary material available at <https://doi.org/10.1038/s42005-023-01502-8>.

Correspondence and requests for materials should be addressed to Ying-Jer Kao.

Peer review information *Communications Physics* thanks Titus Neupert and the other, anonymous, reviewer(s) for their contribution to the peer review of this work. A peer review file is available.

Reprints and permission information is available at <http://www.nature.com/reprints>

Publisher's note Springer Nature remains neutral with regard to jurisdictional claims in published maps and institutional affiliations.



Open Access This article is licensed under a Creative Commons Attribution 4.0 International License, which permits use, sharing, adaptation, distribution and reproduction in any medium or format, as long as you give appropriate credit to the original author(s) and the source, provide a link to the Creative Commons license, and indicate if changes were made. The images or other third party material in this article are included in the article's Creative Commons license, unless indicated otherwise in a credit line to the material. If material is not included in the article's Creative Commons license and your intended use is not permitted by statutory regulation or exceeds the permitted use, you will need to obtain permission directly from the copyright holder. To view a copy of this license, visit <http://creativecommons.org/licenses/by/4.0/>.

© The Author(s) 2024